THE JOURNAL OF BIOLOGICAL CHEMISTRY VOL. 287, NO. 20, pp. 16311–16323, May 11, 2012
Published in the U.S.A.

Activation of Moesin, a Protein That Links Actin Cytoskeleton to the Plasma Membrane, Occurs by Phosphatidylinositol 4,5-bisphosphate (PIP2) Binding Sequentially to Two Sites and Releasing an Autoinhibitory Linker*[S]

Received for publication, September 22, 2011, and in revised form, March 16, 2012 Published, JBC Papers in Press, March 20, 2012, DOI 10.1074/jbc.M111.304881

Khadija Ben-Aissa[‡], Genaro Patino-Lopez[‡], Natalya V. Belkina[‡], Ofelia Maniti[§], Tilman Rosales[¶], Jian-Jiang Hao[‡], Michael J. Kruhlak[‡], Jay R. Knutson[¶], Catherine Picart[§], and Stephen Shaw[‡1]

From the [‡]Experimental Immunology Branch, NCI, and [¶]Laboratory of Molecular Biophysics, NHLBI, National Institutes of Health, Bethesda, Maryland 20892 and the [§]Grenoble Institute of Technology and CNRS, LMGP, UMR 5628, 3 parvis Louis Néel, 38016 Grenoble, France

Background: Phosphatidylinositol 4,5-bisphosphate (PIP2) activates moesin via two binding sites whose roles are poorly understood.
Results: Critical residues are identified in both sites and an inhibitory linker (FLAP) is characterized.
Conclusion: Activation of moesin requires PIP2 binding to each site and release of the FLAP.
Significance: The results fit a sequential activation model involving conformational change and interfacial release of FLAP.

Many cellular processes depend on ERM (ezrin, moesin, and radixin) proteins mediating regulated linkage between plasma membrane and actin cytoskeleton. Although conformational activation of the ERM protein is mediated by the membrane PIP2, the known properties of the two described PIP2-binding sites do not explain activation. To elucidate the structural basis of possible mechanisms, we generated informative moesin mutations and tested three attributes: membrane localization of the expressed moesin, moesin binding to PIP2, and PIP2-induced release of moesin autoinhibition. The results demonstrate for the first time that the POCKET containing inositol 1,4,5-trisphosphate on crystal structure (the "POCKET" Lys-63, Lys-278 residues) mediates all three functions. Furthermore the second described PIP2-binding site (the "PATCH," Lys-253/Lys-254, Lys-262/Lys-263) is also essential for all three functions. In native autoinhibited ERM proteins, the POCKET is a cavity masked by an acidic linker, which we designate the "FLAP." Analysis of three mutant moesin constructs predicted to influence FLAP function demonstrated that the FLAP is a functional autoinhibitory region. Moreover, analysis of the cooperativity and stoichiometry demonstrate that the PATCH and POCKET do not bind PIP2 simultaneously. Based on our data and supporting published data, we propose a model of progressive activation of autoinhibited moesin by a single PIP2 molecule in the membrane. Initial transient binding of PIP2 to the PATCH initiates release of the FLAP, which enables transition of the same PIP2 molecule into the newly exposed POCKET where it binds stably and completes the conformational activation.

The ERM[2] (ezrin, moesin, and radixin) family of proteins is comprised (in vertebrates) of three members having high sequence similarity (1–4). All cells express at least one of the three in high abundance where it functions to link cortical actin to plasma membrane. The structure of the ERM protein consists of three functional regions: 1) a ~300 amino acid N-terminal compound FERM domain (consisting of lobes A, B, and C); 2) a ~200 amino acid linker region that is mostly α-helical; and 3) a ~70 amino acid C-terminal tail (Fig. 1*A*). ERM proteins undergo conformational inter-conversion between an active conformation and an inactive conformation. In the active conformation (Fig. 1*B*) the ERM protein is located at the membrane where the FERM domain binds to multiple ligands, the linker region is an extended helix, and the C-terminal tail binds to actin cytoskeleton. FERM binding to protein ligands occurs via two binding sites: a "hydrophobic groove," which binds to tails of transmembrane proteins, such as CD44 (5) (Fig. 1*B*, *site 3*); and a hydrophobic helix-binding site for short α-helices such as NHERF1 and NHERF2 (6) (Fig. 1*B*, *site 4*). In the inactive conformation (Fig. 1*C*) the ERM protein is autoinhibited and located in the cytosol. In that conformation much of the surface area of the FERM domain (including sites 2, 3, and 4) is masked by multiple parts of the linker and C-terminal tail (7, 8). This autoinhibition involves masking both major protein binding sites on the FERM domain.

* This work was supported, in whole or in part, by the National Institutes of Health Intramural Research Programs of the NCI and NHLBI and Agence Nationale de la Recherche (ANR-08-PCVI-026) and by the European Research Council (GA259370).
[S] This article contains supplemental Figs. S1 and S2.
[1] To whom correspondence should be addressed: Experimental Immunology Branch, NCI, National Institutes of Health, Bethesda, MD 20892. Tel.: 301-435-6499; Fax: 301-496-0887; E-mail: Shaws@mail.nih.gov.

[2] The abbreviations used are: ERM, ezrin, moesin, and radixin; PIP2, phosphatidylinositol 4,5-bisphosphate; IP3, inositol 1,4,5-trisphosphate; BisTris, 2-[bis(2-hydroxyethyl)amino]-2-(hydroxymethyl)propane-1,3-diol; LUV, large unilamellar vesicle; PH, pleckstrin homology; PE, phosphatidylethanolamine; PC, phosphatidylcholine; PS, phosphatidylserine; dansyl, 5-dimethylaminonaphthalene-1-sulfonyl.

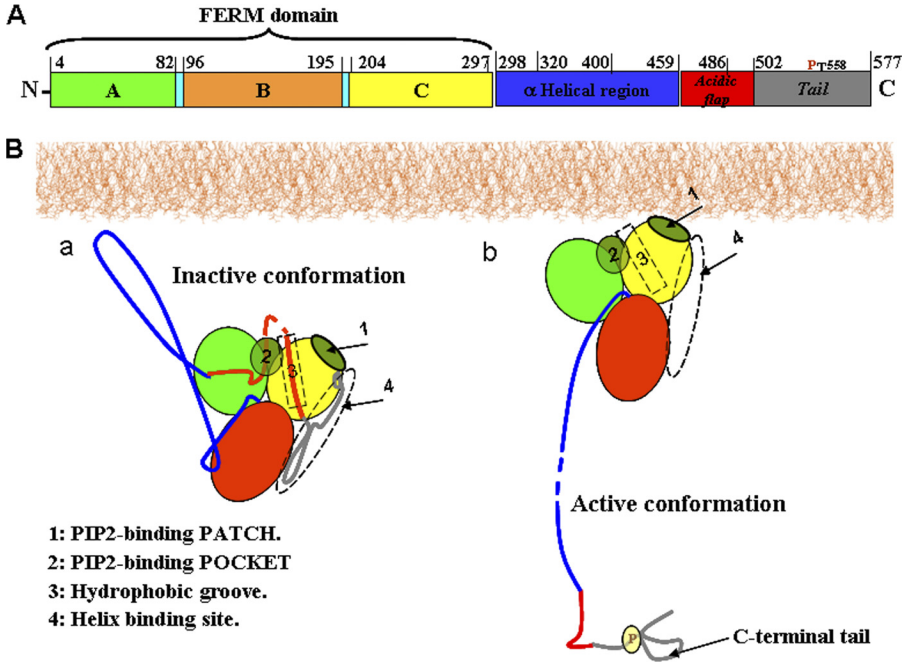

FIGURE 1. **Moesin domain organization, conformational states, and binding sites.** Correspondence between regions of sequence and the domain architecture of full-length moesin. Colors correspond to distinct functional parts: lobe A of FERM domain (*green*), lobe B (*orange*), lobe C (*yellow*), α-helical region (*blue*), FLAP (*red*), and C-terminal tail (*gray*). *A,* domains of moesin within the primary sequence. Residue numbers in human moesin are shown for boundaries and for the C-terminal phosphorylation site. *B*, schematic of full-length inactive and active conformations. Also shown in *light blue* and labeled in the figure are four known binding sites of the ERM protein that include two for PIP2 (*1* and *2*) and two for protein ligands (*3* and *4*). The two PIP-2 binding sites are shaded *dark green*. The two protein-binding sites are enclosed with *dashed regions*. *a,* schematic of inactive conformation (based on structure 2I1K) in which three binding sites are masked (by α-helical region, FLAP, and tail) but the PIP2-binding lysine PATCH (*1*) remains exposed. (The connecting peptide between the FLAP and C-terminal tail is poorly visible because it runs behind lobe C in this perspective.) *b,* schematic of active conformation in which three of the binding sites are unmasked. The helical region is shown with *dashes in the middle* to indicate it is longer than shown.

ERM activation is dynamically regulated and critical to processes as diverse as mitosis (9), platelet activation (10), and *Drosophila* wing disk development (11). A major challenge is to understand the mechanism(s) that mediates conformational activation of the ERM protein. Binding to membrane phosphatidylinositol 4,5-bisphosphate (PIP2) is understood to be the dominant mode of activation of ERM. Tsukita and colleagues (12) first showed that full-length ERM proteins bound to PIP2. To test whether PIP2 was able to activate the ERM protein they tested whether PIP2 influenced binding of the ERM protein to CD44. They showed that PIP2 induces conformational activation of ERM proteins, which enables them to bind to CD44. PIP2 binding to ERM proteins and their activation is critical to their localization and function at the membrane. This was first proven by studies showing impaired ERM localization at the membrane caused by microinjection of the polyphosphoinositide-binding agent neomycin (13) and later confirmed by acute reduction of membrane PIP2 (14). In addition to activation by PIP2, phosphorylation of a conserved threonine on the C-terminal tail also contributes to activation. However, this phosphorylation is believed to stabilize the active state after PIP2 rather than to initiate activation (15).

What is the molecular mechanism by which PIP2 mediates conformational activation of the ERM proteins? Current understanding is incomplete and complicated by evidence of two binding sites. One site, the "PIP2-binding POCKET" (the POCKET), was clearly identified in a crystal structure of the radixin FERM domain in complex with IP3 (16). It is located in a cleft between lobe A and lobe C in the FERM domain (Fig. 1*B*, *POCKET*). The authors proposed that PIP2 binding to this site caused long range conformational changes of the FERM domain that promotes release of the ERM C terminus. Independently a distinct PIP2-binding site on the surface of lobe C (the PATCH) was described by Niggli and colleagues (17) based on its functional importance in mediating binding to PIP2 and membrane localization of the cellular ERM protein. They predicted that primary sequence motifs with adjacent lysines could mediate PIP2 binding and identified two candidate pairs of lysines on the surface of lobe C (Lys-253/Lys-254 and Lys-262/Lys-263) (Fig. 1*B*, the PATCH). Combined mutation of all four residues to asparagines ("the 4N mutant") virtually destroyed FERM domain binding to PIP2. Their role in binding PIP2 has been established for the FERM domain (17) and for the intact ERM protein (11). These residues are critical for ERM localization at the membrane (14, 16, 17).

Lobe C, which contains the aforementioned PATCH, is a PH-like domain. PH-like domains have a conserved composite-fold consisting of two β sheets packed against each other with a single helix capping the orifice of the resultant partially open barrel (18, 19). This conserved scaffold has been widely utilized in diverse proteins to perform a range of biochemical functions because the overall β-barrel-fold provides several distinct niches for potential interactions with substrates. PH domains are particularly known for their capacity to bind membrane phospholipids (especially PIP2) via conserved lysine or arginine residues in a positively charged pocket formed at the opening of the β barrel (20–24). However, that POCKET in lobe C is unavailable for PIP2 binding because it is a hydrophobic pocket

used for binding the extreme C-terminal helix of ERM protein (Fig. 1*B*, *C site 4*). Instead the lysine pairs in the PATCH are on loops of a β sheet ($\beta5/\beta6/\beta7$) approximately where Pearson noted a patch of positive electrostatic charge that he proposed might be a PIP2-binding site (8). This proposed location for PIP2 binding has not been observed in solved structures of PIP2 binding PH domains.

There are major missing pieces in our understanding of the two PIP2-binding sites and in understanding the functional relationship between them. Regarding the POCKET there are two key issues. First, its functional relevance is largely untested experimentally. Second, the recently solved structure of full-length autoinhibited ERM raises a new conceptual problem by showing that the POCKET is masked by a linker region (Figs. 1*C* and 7*A*) "hindering PIP2 and membrane interactions" (7). Consequently, it is problematic to propose that this site mediates the initial PIP2 binding. Regarding the PATCH it is not clear whether it simply mediates PIP2 binding or also mediates release of autoinhibition.

Therefore, we have undertaken a systematic study of the structural basis of PIP2 binding to develop a model of the sequence of events in moesin activation by binding to PIP2. Our evidence indicates that the PATCH mediates not only the initial binding to PIP2, but more importantly results in the PIP2-induced conformational activation of ERM protein. That activation involves release of an autoinhibitory "FLAP," which we characterize.

EXPERIMENTAL PROCEDURES

Cells and Reagents—All lipids were synthetic, unless otherwise indicated. POPC (PC; 1-palmitoyl-2-oleoyl-*sn*-glycero-3-phosphocholine), phosphatidylethanolamine (PE; 1-palmitoyl-2-oleoyl-*sn*-glycero-3-phosphoethanolamine), POPS (PS; 1-palmitoyl-2-oleoyl-*sn*-glycero-3-phosphoserine), L-α-phosphatidylinositol natural from bovine liver, $PI(4,5)P_2$ (PIP2; L-α-phosphatidylinositol 4,5-bisphosphate) natural from porcine brain, and sphingomyelin natural from brain were all purchased from Avanti Polar Lipids. Cholesterol (purified from sheep wool grease) was purchased from Sigma. Dansyl-PE (*N*-[5-(dimethylamino)naphthalene-1-sulfonyl]-1,2-dihexadecanoyl-*sn*-glycero-3-phosphoethanolamine) was obtained from Molecular Probes. Anti-His antibody was purchased from Abcam. Jurkat WT cells (from ATCC) were grown in RPMI 1640 (Invitrogen) containing L-glutamine and 25 mM HEPES, with 10% FBS (HyClone).

DNA Constructs—The GFP-tagged construct of full-length human moesin was prepared in pEGFP-N1 vector (Clontech) as described previously (14). Mutant constructs were generated using the QuikChange site-directed mutagenesis kit (Agilent Technologies). Moesin tagged with Myc-His_6 at its C terminus were prepared by cloning the coding DNA into XhoI and HindIII sites of the expression vector pBAD-Myc-His (Invitrogen). Similar techniques were used to add a linker of two glycines and a cysteine after the C terminus of moesin in those constructs for the purpose of fluorescent labeling. All constructs and mutations were verified by DNA sequencing. The GST-tagged proteins (CD44 tail (residues 291–361), NHERF1 tail (residue 347–358), and NHERF1 full-length) were generated by producing DNA fragments by reverse transcription-PCR with primers encoding the corresponding region, using total mRNA isolated from human peripheral blood T-cells and subcloned into BamHI and SalI sites of pGEX-4T-2 (GE Healthcare).

Cell Transfection and Immunofluorescence Analysis—Cells were transfected with 10 μg of each plasmid in a BTX ECM 830 electroporator (Harvard Apparatus, 300 V for 10 ms). After incubation at 37 °C for 16 to 24 h the cells were adjusted to 10^7 cells/ml in Hanks' balanced salt solution containing 0.3% BSA, 200 μl were added onto poly-D-lysine-precoated glass bottom of 35-mm culture dishes (MatTek). The cells were allowed to settle for 10 min at 37 °C, then fixed by the addition of 1.0 ml of 4% paraformaldehyde solution. After 10 min at room temperature, the cells were washed four times with PBS and examined using a Zeiss LSM510 laser scanning confocal microscope using a ×63 (N.A. 1.4) or ×100 (N.A 1.4) plan-apochromat oil immersion objective lens (Carl Zeiss). Quantitative analysis was performed using the Imaging Examiner software (LSM, Carl Zeiss, Inc.) and for display purposes the contrast for the GFP fluorescence images was inverted using Adobe photoshop software. For each cell analyzed, a line was drawn manually at the plasma membrane, and another line was drawn just inside the plasma membrane in the cytosol as described previously (14, 23). The average fluorescence intensity was determined for the set of pixels of the plasma membrane line (plasma membrane mean intensity) and for the set of pixels at a cytosol line (cytosol mean intensity). Membrane enrichment for each cell was calculated as the (plasma membrane mean intensity)/(cytosol mean intensity) and expressed as the mean ± S.E. of at least 10 representative cells from three independent experiments.

In Vitro Pulldown Assay—Recombinant proteins were produced in bacteria and purified using GST or His tags as previously described (14). Pulldown assays were performed with His-tagged moesin constructs and GST-tagged NHERF1 or CD44 constructs as described previously (14). In brief, for each reaction 1 μM of the indicated purified His-protein was mixed with 5 μM of the indicated GST proteins bound to the glutathione-Sepharose 4B beads. Each reaction was done in the presence or absence of 50 μg/ml of PIP2 or PS phospholipids (Avanti Polar Lipids, Inc.) in buffer A (20 mM Tris-HCl, pH 7.5, 1 mM EGTA, 150 mM NaCl, 1 mM DTT, and 0.05% Tween 20). The mixture was incubated for 90 min at 4 °C under constant rotation. After centrifugation at 600 × *g* for 3 min, the pellet was washed three times with buffer A, and diluted in SDS buffer twice. Samples from each reaction were run into two NuPAGE BisTris gels (Invitrogen). One gel was transferred into PVDF membrane and the bound His protein was revealed by immunoblotting using anti-His antibody (Abcam). The other gel was stained with Coomassie Blue to confirm equal loading of GST proteins. All results shown are representative of at least 3 pulldown experiments.

Lipid Cosedimentation Assay—Large unilamellar vesicles (LUVs) were prepared as described previously (25). Briefly, mixtures of lipids PC/PIP2 (95/5% unless otherwise indicated) or PC/PS (80/20%) were prepared, dehydrated under a stream of nitrogen, and dried further overnight in a SpeedVac. Dried lipid films were hydrated in a HEPES buffer containing: 20 mM HEPES, 200 mM sucrose, 0.5 mM EDTA, pH 7.4, for 2 h at 37 °C

accompanied by rigorous vortexing each 15 min, and then underwent 5 thaw/freeze cycles. The lipids were sonicated and passed 25 times through two 100-nm pore size polycarbonate membranes of a mini-extruder (Avanti Polar Lipids). Purified moesin-GGC-myc His wild type and mutants were labeled using Alexa 488-C5-maleimide (Molecular Probes) as described (25). The ratio of Alexa 488 incorporated per mol of each moesin proteins was (0.5–0.8):1.

The affinity of fluorescently labeled moesin and mutants for sucrose-loaded PIP_2-LUVs was determined by sedimentation assays in a HEPES-KCl buffer (20 mM HEPES, pH 7.4, 100 mM KCl, 0.5 mM EDTA). The co-sedimentation assays used a series of assays varying the concentration of total lipids, whereas keeping the total protein concentration constant at 400 nM. After incubation for 15 min at room temperature, the 100-μl samples were centrifuged at 16,000 $\times$ g for 1 h and 30 min at 4 °C using an Eppendorf 5810R centrifuge. The top 80 μl of each sample were removed and considered as supernatant. 10 μl of Triton X-100 and 60 μl of KCl buffer were added to resuspend the pellet. The intensities of supernatant and pellet samples were read in a fluorescence microplate reader (Infinite 1000, Tecan Austria) with excitation and emission set, respectively, at 490/521 nm ($\pm$5 nm). The percentage of bound protein was calculated as previously described (25).

Moesin to Membrane PIP2 FRET Stoichiometry Titration—PIP2 stoichiometry titration was carried out using an established protein to membrane FRET assay (26). Briefly, LUVs were made using a lipid mixture of PE/PC/PS/L-α-phosphatidylinositol/sphingomyelin/cholesterol/dansyl-PE/PIP2 (23.8:9.1:18.1:4.5:4.5:25:5:10) to mimic the physiological membrane lipid composition as previously described (26). Samples contained purified moesin protein (3.6 μM) and 10 μM free Ca^{2+} in physiological buffer (25 mM HEPES, pH 7.4, 140 mM KCl, 15 mM NaCl, 0.5 mM $MgCl_2$, and 15 mM EDTA). PIP2 LUVs (10% PIP2) were titrated into protein solution, and the protein to membrane FRET was measured with a spectrofluorimeter (HORIBA, SPEX FLUOROG 321) at 25 °C, with excitation and emission slits at 4 and 8 nm, respectively. Intrinsic donor tryptophan residues in moesin were excited at 284 nm and emission at 522 nm from dansyl-PE acceptor residues was quantitated. To correct for direct acceptor excitation, we subtracted the background dansyl fluorescence of a control sample lacking protein from experimental samples. The data were analyzed using linear least squares fitting of the rise phase and the saturation phase such that the stoichiometry was defined by the intersection of these two straight lines relative to the molar amount of protein used in the assay.

Analysis of Structure—The solved structure of full-length closed ERM 2I1K (7) and radixin FERM domain 1GC7 (16) were obtained from the Protein Data Bank. To reconstitute the missing loops in full-length moesin (amino acids 320–326, 399–410, and 472–486) loop searches were performed followed by optimization of the molecular coordinates of the atoms by potential energy minimization using Sybyl 7.0 (Tripos, St. Louis, MO) with AMBER Force Fields (FF99) parameters. Surface electrostatic potentials were rendered using the MOLCAD subroutine of Sybyl with the AMBER7 FF99 charge set, which has an unconventional color scheme but provides a particularly robust calculation of electrostatic potentials. Structures alignment and root mean square deviation calculations were performed by using VMD (developed with NIH support by the Theoretical and Computational Biophysics group at the Beckman Institute, University of Illinois at Urbana-Champaign).

RESULTS

The PIP2 Binding POCKET Is Necessary for ERM Activation—To better characterize the functional importance of the PIP2-binding POCKET in full-length moesin and the residues critical for its function, we generated mutant moesin constructs and assayed the resulting protein for multiple functions. In the solved structure of the Radixin FERM-IP3 complex (1GC6) three lysines (Lys-60 and Lys-63 from lobe A and Lys-278 from lobe C) were predicted to contact the three phosphate groups of IP3 (Fig. 2*A*). We generated mutant moesin constructs in which each of these lysines was substituted individually with asparagine, which reduces the positive charge but otherwise preserves most of the side chain of the residue. ERM protein localization at the plasma membrane requires PIP2 (13, 14), we therefore screened the functional importance of individual residues by assessing the affect of mutations on plasma membrane enrichment of moesin constructs tagged with GFP at their C terminus. Note that localization of the GFP-tagged protein is similar to native moesin in fibroblasts (27) and Jurkat T-cells (supplemental Fig. S1). Wild type (WT) moesin was present in the cytoplasm but visibly enriched at the membrane (Fig. 2*B*). Fluorescence images demonstrated differences in the degree of enrichment at the plasma membrane among the constructs. To objectively assess the change, we measured the localization at the membrane (relative to cytosol) for each protein and compared it to the membrane localization of the native protein (Fig. 2*C*). The results demonstrated that individual mutations of K63N and K278N each reduced membrane localization by more than 50%, which is consistent with their functional role in PIP2 binding inferred from the structure. In contrast K60N augmented membrane localization, indicating that Lys-60 was not a critical facilitator of membrane binding. A double mutation of K63N/K278N reduced membrane localization by more than 80% (Fig. 2*C*).

Mutation of POCKET Impairs PIP2 Binding and PIP2-induced Activation—To confirm that Lys-63 and Lys-278 in intact moesin form a binding site for PIP2 *per se* we examined PIP2-binding to WT and K63N/K278N in an *in vitro* cosedimentation assay. The PIP2 cosedimentation assays (25) were performed using a constant concentration of moesin WT or mutant K63N/K278N and different concentrations of LUVs containing 95% phosphatidylcholine (PC) and 5% of the acidic phospholipid PIP2. The results show that compared with WT (K_d = 22.3 $\pm$ 2.6 μM) the mutation K63N/K278N markedly decreased the binding of moesin to PIP2 (K_d = 105.6 $\pm$ 8.6 μM) (Fig. 3*A*).

We assessed whether the POCKET is essential for PIP2-induced conformational activation of moesin in a pulldown assay using protein ligands CD44 tail and NHERF-1 tail. As expected, PIP2 is required for induction of WT moesin binding to CD44 (Fig. 3*B*) and strongly augments WT moesin binding to

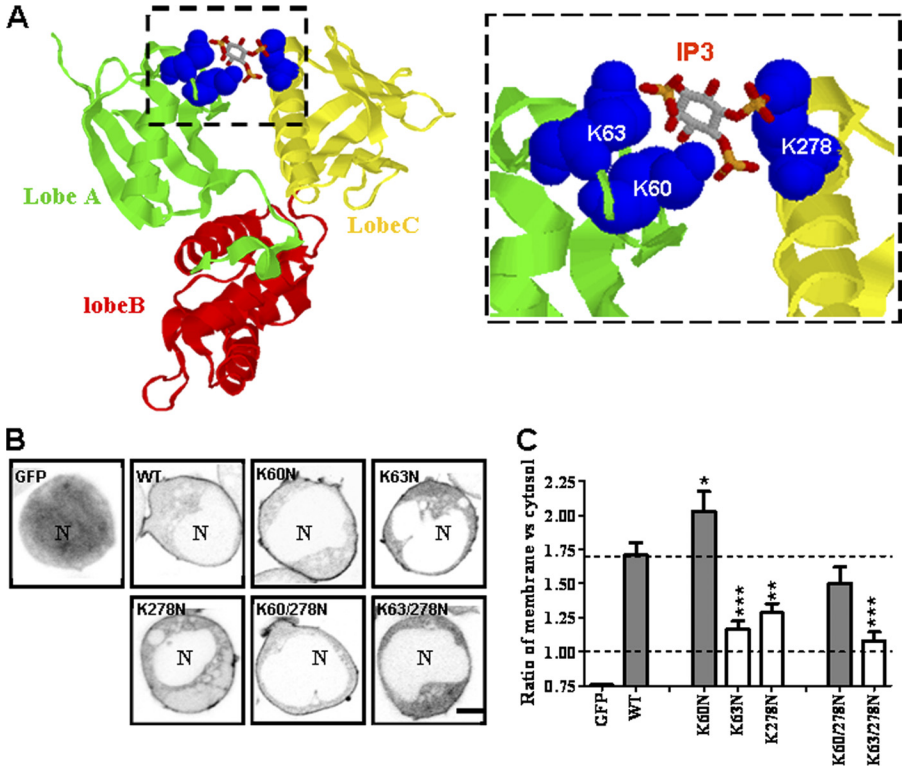

FIGURE 2. **The PIP2 binding POCKET defined by crystallography is necessary for ERM activation.** *A,* the complex of radixin FERM domain with IP3 (PDB 1GC6) represented as ribbon drawing. The *dashed box* highlights the basic cleft between lobes A and C. The IP3 molecule is shown in a *ball and stick* model. The positively charged residues proposed to interact with the phosphate groups of IP3 are shown in *space-filled* and *colored blue*. The side chains of IP3 are shown in *ball-and-stick* models. *Inset* shows expanded view of this cleft. *B,* membrane enrichment of GFP-tagged constructs of WT or mutant moesin (and GFP-only as control) was assessed in representative midplane confocal images of transfected Jurkat cells. The large nucleus of Jurkat is indicated with "N." *Scale bar* is 5 μm. *C,* quantitation of membrane enrichment of moesin constructs in Jurkat cells having the indicated mutations of lysines in the PIP2-binding POCKET. The enrichment characteristic of the WT protein is indicated by the *upper dashed line*. Proteins not enriched at the plasma membrane typically have ratios of membrane/cytoplasmic localization of ~1.0 (*lower dashed line*). Statistical significance compared with Moesin WT membrane enrichment is shown as: *, $p < 0.1$; **, $p < 0.01$; ***, $p < 0.001$.

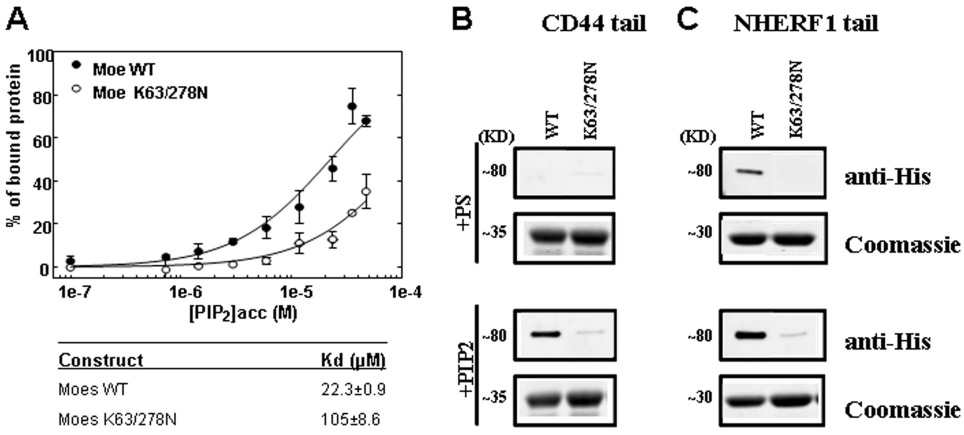

FIGURE 3. **Mutation of the PIP2 POCKET abolishes PIP2 binding.** *A*, binding of WT and K63N/K278N moesin to PIP2 in LUV was measured by a cosedimentation assay over the indicated range of PIP2 concentrations. Dissociation constants (mean of two independent experiments ± S.D.) are presented in the *lower panel*. *B* and *C*, binding of moesin to the cytoplasmic tail of CD44 (*B*) and the tail of NHERF1 (*C*) were assessed by pulldown assays. Recombinant proteins WT and K63/278N moesin were tested in the presence of lipid control PS (phosphatidylserine) (*upper panels*) or PIP2 (*lower panels*). Regions shown are from the pellet using anti-His to detect moesin pulled down and Coomassie stain to validate equal loading of GST-CD44 or GST-NHERF1.

NHERF1 (Fig. 3*C*). In contrast, K63N/K278N moesin is severely deficient in PIP2-induced binding to CD44 and NHERF1.

PATCH Lysines Are Individually Critical for Membrane Localization of ERM Proteins—We undertook similar characterization of the second described PIP2-binding site on the ERM protein to confirm which residues are critical and the roles they play in PIP2 binding and activation. Barret *et al.* (17) identified a set of four lysines (consisting of two pairs Lys-253/Lys-254 and Lys-263/Lys-264) that are required for PIP2 binding to the isolated FERM domain. The choice of Barret *et al.* (17) of residues to mutate was based on motifs in primary sequence (because no solved structure was then available). With the benefit of a solved structure (7), it is now apparent that

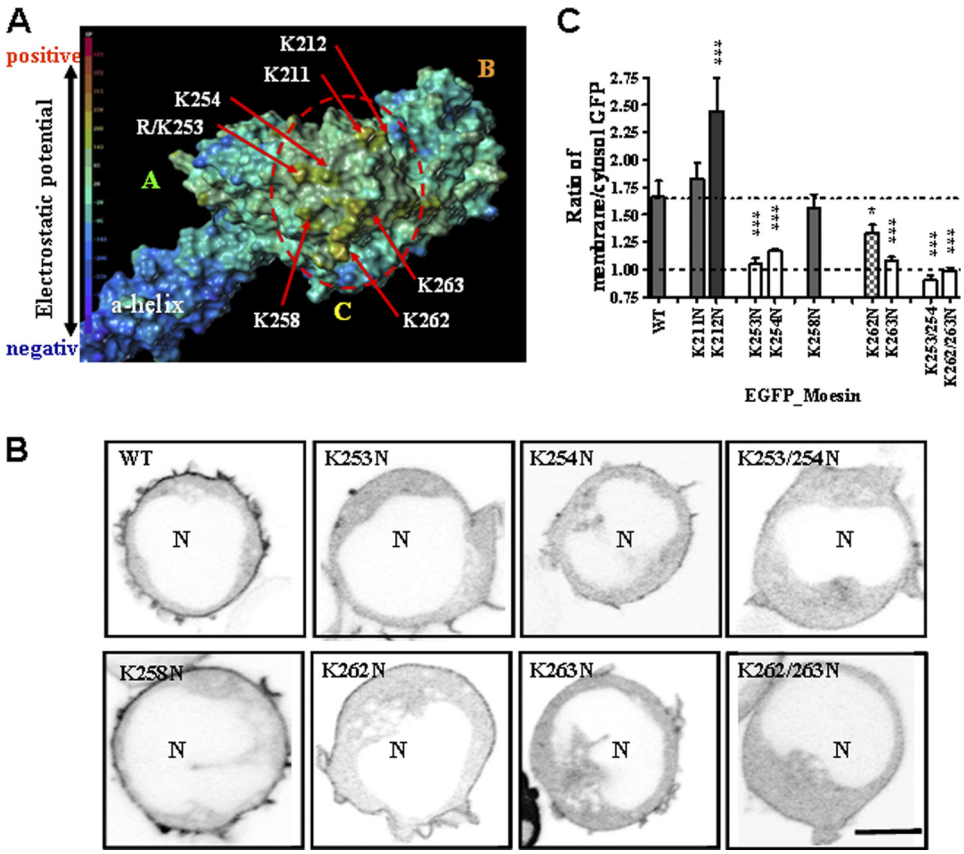

FIGURE 4. **The PATCH of four lysines is critical for membrane localization of ERM protein.** *A,* electrostatic surface potential of full-length insect ERM protein (PDB 2I1K) with color charge scale on the *left*. The molecule is oriented to show the single area of highest positive charge on the entire molecule (*dashed circle*). Labels indicate locations of the *A*, *B*, and *C* lobes. Location and identity of positively charged resides in the area are indicated. *B,* membrane enrichment of GFP-tagged constructs of WT or mutant moesin was assessed in representative midplane confocal images of transfected Jurkat cells. The large nucleus of Jurkat is indicated with *N*. *Scale bar* is 5 μm. *C,* quantitation of membrane enrichment of moesin constructs in Jurkat cells. The enrichment characteristic of the WT protein is indicated by the *upper dashed line*. Proteins not enriched at the plasma membrane typically have ratios of membrane/cytoplasmic localization of ~1.0 (*lower dashed line*). Statistical significance compared with Moesin WT membrane enrichment is shown as: *, $p < 0.1$; **, $p < 0.01$; ***, $p < 0.001$.

those four lysine residues are exposed on the surface of lobe C with a relatively high positive charge surface potential, which should be favorable for interaction with the negatively charged phosphate of PIP2. In addition to these four, three other lysines are present in that vicinity (Lys-211, Lys-212, and Lys-258) (Fig. 4*A*). To assure comprehensive evaluation of potentially relevant residues, we expanded the analysis to include all seven positively charged residues in the area of the strong positive electrostatic charge on the surface of lobe C (Fig. 4*A*).

We generated mutant moesin constructs in which each of these lysines were substituted individually with asparagine and assessed their enrichment at the plasma membrane in Jurkat-transfected cells. The results (Fig. 4, *B* and *C*) clearly demonstrate that three of these lysines were most critical for membrane localization: Lys-253, Lys-254, and Lys-263 (Fig. 4*C*). A fourth residue, Lys-262, was less critical, but its mutation to Asn also reduced membrane localization. The four important lysines are precisely the two pairs of adjacent lysines identified by Barret: Lys-253/Lys-254 and Lys-262/Lys-263 (17). Double mutation of either pair strongly decreases membrane localization (Fig. 4*C*). Mutations of two nearby lysines (Lys-258 and Lys-211) did not influence membrane association and one mutation (K212N) augmented membrane association, confirming that not all lysines in the vicinity behave similarly. (This property of the K212N mutation most likely reflects the role it plays in stabilizing autoinhibition by the tail, because it binds to the α-carboxylate group of the C-terminal residue (8, 28)).

Single Mutations within PATCH Do Not Impair PIP2 Binding—It is notable that *single* mutations of critical lysines impair membrane localization. Previously, the only ERM protein constructs demonstrated to have impaired membrane localization were those having mutations of all four lysines (K253N/K254N/K262N/K263N). To check whether the impairment of the localization of the single mutants at the plasma membrane is related to a defect in PIP2 binding we assessed PIP2 binding directly using an *in vitro* cosedimentation assay (similar results were obtained with fluorescence correlation spectroscopy studies (data not shown)). Most of the moesin proteins having single mutations and double mutations did not have gross defects in binding to PIP2 (Fig. 5). In contrast, simultaneous mutation of the four lysines (4N) decreases strongly the binding to PIP2 containing LUVs (Fig. 5).

Single Mutations within PATCH Impair PIP2-induced Activation—The foregoing data demonstrate that single mutations impair membrane localization without major impairment of PIP2 binding. Thus, membrane localization appears to depend on more than simply PIP2 binding. We hypothesized that the additional requirement might be the need for PIP2-

mediated conformational activation. We investigated moesin binding to the tail of CD44 in a pulldown assay in the presence of PIP2 or a control lipid PS. Each of the three mutants that were severely impaired in membrane localization were also deficient in PIP2-induced binding to CD44 (Fig. 6*A*) and NHERF1 tail (Fig. 6*B*). For both the CD44 (Fig. 6*A*) and NHERF1 tails (Fig. 6*B*), the K262N mutant ERM had only mildly reduced PIP2-induced binding, consistent with its mildly reduced membrane localization (Fig. 4*C*). To further assess this apparent mild defect, we tested an additional ligand, full-length NHERF1, whose binding to the ERM protein is less avid because of NHERF1 intramolecular autoinhibition (29). Using this more stringent probe (Fig. 6*C*), the defect in the K262N mutant is clearly evident. Thus, the mutant moesin proteins have lost PIP2-induced conformational exposure of two distinct binding sites: the hydrophobic groove that binds CD44 tails and the helix binding site, which binds NHERF1 (Fig. 1*B*). Also, note that even though these mutants still bind to PIP2 they are defective in functional activation by PIP2.

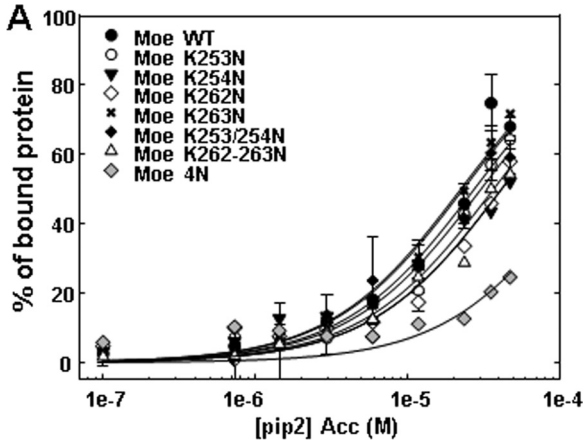

B

Construct	Kd (μM)
Moes WT	22.3±2.6
Moes K253N	30.3±4.0
Moes K254N	36.7±4.2
Moes K262N	41.4±5.9
Moes K263N	23.2±2.8
Moes K53/254N	27.4±3.6
Moes K262/263N	41.4±5.6
Moes 4N	135±25.5

FIGURE 5. **Binding of PATCH mutant constructs to PIP2.** *A*, binding of WT and mutant moesin to PIP2 in LUV was measured by a cosedimentation assay over the indicated range of PIP2 concentrations. Moesin constructs tested included WT, each of the single lysine mutations (K253N, K254N, K262N, K263N), and double mutations of the two pairs (K253N/K254N and K262N/K263N) that strongly impaired membrane localization in cells and the combined mutation of the 4 lysines K253N/K254N/K262N/K263N (4N). *B*, tabulation of dissociation constant (mean of two independent experiments ± S.D.).

FLAP Contributes to Autoinhibition—The foregoing results confirm the existence of two spatially distinct PIP2-binding sites and demonstrate that each is necessary for moesin activation by PIP2 and for membrane localization in cells. However, examination of the crystal structure of full-length ERM protein shows that these two sites are very different in accessibility. The PATCH is exposed at the surface and has an electrostatic potential favorable to interaction with PIP2 (Fig. 4*A*). In contrast the POCKET is largely masked by a linker region, which was clearly seen when the structure of full-length insect ERM was resolved (7). It is a short acidic region of about 23 amino acids (472–494) that masks the hydrophobic groove (which binds CD44) and the PIP2-binding POCKET (Fig. 7*C*). Because this region has not previously been named, we refer to it as the FLAP based on its properties described herein. Moreover, the presence of the FLAP overlaying the POCKET reverses its electrostatic surface potential. In the unmasked FERM domain the POCKET has a high positive electrostatic surface potential favorable for interaction with negatively charged membrane phospholipid headgroups (Fig. 7*B*). In contrast in the full-length autoinhibited moesin the electrostatic surface potential of the POCKET becomes negative and nonfavorable to interact with membrane phospholipids (Fig. 7*A*).

To appreciate the potential role of the FLAP in regulating ERM function we explored its sequence conservation and its

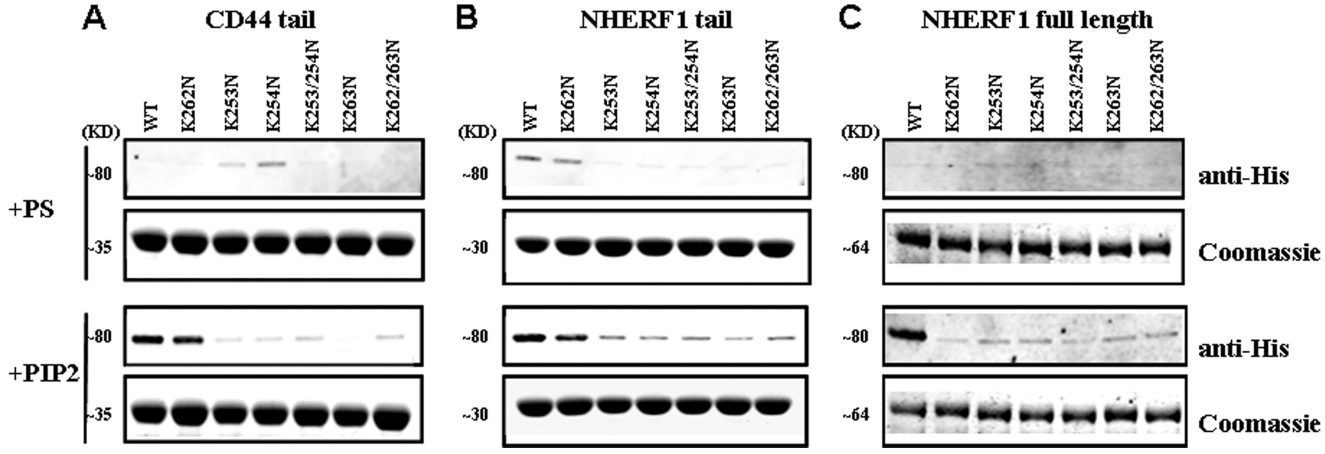

FIGURE 6. **Single lysine mutations in the PATCH impair PIP2-induced activation of moesin binding to CD44 and NHERF1.** *A*, binding of moesin to CD44 was assessed using pulldown of moesin-His by CD44 tail-GST immobilized on beads. Moesin constructs tested included WT, each of the single lysine mutations that strongly impaired membrane binding in cells, and combined mutations of lysines in a pair. Gel regions shown are from the pellet using anti-His to detect moesin pulled down and Coomassie stain to validate equal loading of GST-CD44. *B* and *C*, similar analysis as *A* but using NHERF1 tail-GST (*B*) or NHERF1 full-length-GST (*C*) instead of CD44-GST.

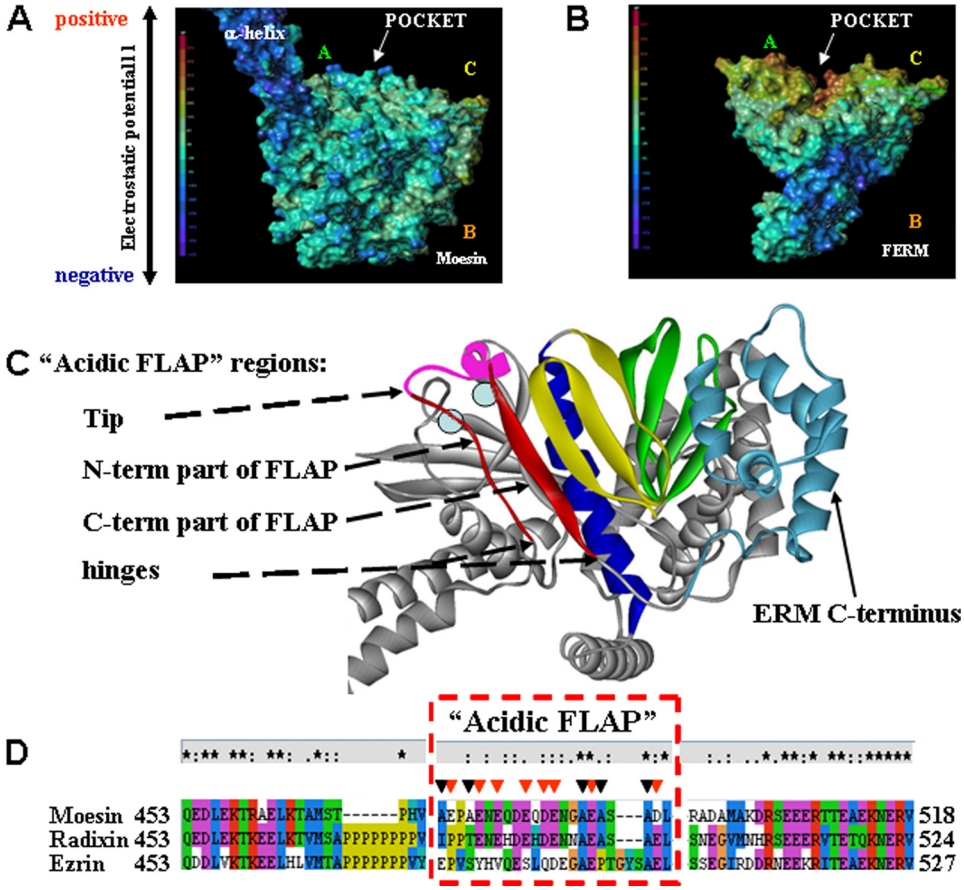

FIGURE 7. **FLAP, sequence and structure analysis.** *A*, electrostatic surface potential of full-length insect ERM protein (PDB 2I1K) and *B*, of unmasked moesin FERM domain with color charge scale on the *left*. The molecules are oriented to show the PIP2 binding POCKET, which is covered by the FLAP in the closed conformation of moesin (*A*) and uncovered in the FERM domain (*B*). Labels indicate locations of the *A*, *B,* and *C* lobes. Location of PIP2 binding POCKET is indicated by *arrows*. *C*, ribbon representation of the closed ERM structure. FLAP is *red* (N-terminal and C-terminal parts) or *magenta* (reconstructed tip, amino acids 473–485). β1 to β4 strands of the PH-like domain are *green*; β5-β7 strands are *yellow*; α-helix is *blue*. C-terminal tail is *light blue*. *Light Blue circles* indicate locations of the two critical residues, Lys-63 and Lys-278, in the POCKET, which are masked by the FLAP when moesin is closed. *D*, multiple sequence analysis of the FLAP of human ezrin, radixin, and moesin and flanking regions. *Red dashed rectangle* highlights the FLAP. *Above* the sequence is a row of symbols that scores the extent of sequence conservation scored by ClustalX (* = identity; : = all residues belong to a strong conservation group; · = all residues belong to a weak conservation group). *Arrowheads* indicate residues in moesin that are acidic (*red*) or short side chains (*black*). Statistical significance compared with Moesin WT membrane enrichment is shown as: *, $p < 0.1$ and **, $p < 0.01$.

features in the x-ray structure. The FLAP is the ONLY region of ERM proteins that shows poor sequence conservation among the three human paralogs (Fig. 7*D*). The two gaps shown in the vicinity of the FLAP are the only ones present in alignments of the full-length ERM proteins. Despite the weak sequence similarity between the FLAP of the paralogs (and orthologs, data not shown), there are two characteristics that are conserved: many acidic residues and scarcity of residues capable of hydrophobic interactions (few Val, Leu and multiple Ala, Gly, and Ser). Examination of this region in PDB 2I1K reveals that the FLAP is loosely associated with the FERM domain. This is evident from the fact that the residues in the loop have an increased B-factor (average 59, compared with average of 41 for the whole structure). The B-factor, also called "temperature factor," is a measure of how much the position of an atom deviates from that given in the atomic coordinates. This deviation is mostly due to thermal motion and reflects the mobility of an atom. The tip of the FLAP is so mobile in the autoinhibited ERM that it is not resolved in the structure.

We undertook mutational analysis to test the hypothesis that the FLAP is a functionally important autoinhibitory region. A construct was designed in which only 23 residues were deleted (472–494); the location and size of the deletion was designed to allow the C terminus (the tail) to associate normally with the FERM domain despite the deletion. The ΔFLAP construct expressed in Jurkat cells showed markedly enhanced localization to the plasma membrane (Fig. 8*A*).

Deletion of the FLAP is a major mutation, and although it was carefully designed to minimize changes elsewhere in the protein, there is always concern that it could influence the structural stability and fold of the entire protein. It was reassuring that ΔFLAP showed no evidence of such abnormalities in binding assays (see below). Nevertheless, we sought a more conservative approach, a point mutation that would loosen binding of the FLAP to the FERM domain. FLAP-FERM binding is maintained by electrostatic and hydrophobic interactions. Analysis of limited hydrophobic interaction of the FLAP with the FERM domain in the autoinhibited structure indicated that residue Leu-281 in the FERM domain interacts with a backbone carbon of the FLAP. Moesin protein with a L281A mutation resembles the ΔFLAP in its enhanced membrane localization (Fig. 8, *A* and *B*). We hypothesized that conversely,

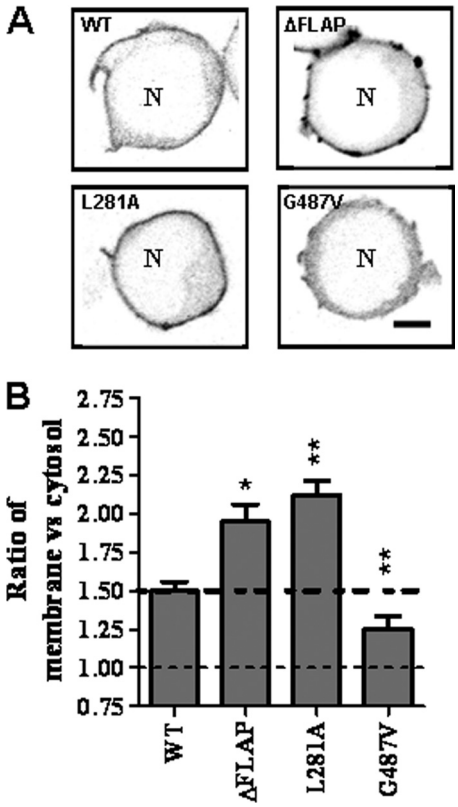

FIGURE 8. **Role of the FLAP in membrane localization of ERM protein.** *A*, Jurkat cells were transfected with GFP-tagged Moesin WT and mutants (FLAP deleted (ΔFLAP), L281A and G487V) followed by fluorescence quantitation as described in the legends to Figs. 2 and 4 (*B*). The enrichment characteristic of the WT protein is indicated by the *upper dashed line*. Proteins not enriched at the plasma membrane typically have ratios of membrane/cytoplasmic localization of ~1.0 (*lower dashed line*).

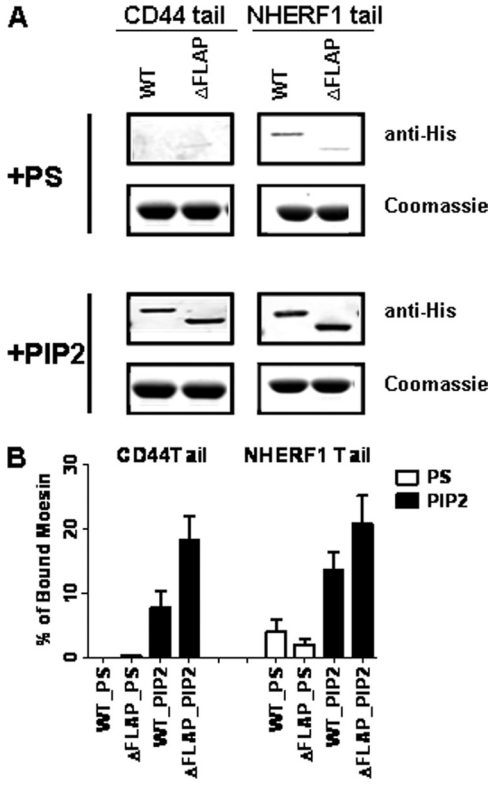

FIGURE 9. **FLAP removal increases PIP2-induced protein ligands binding to moesin.** *A*, SDS-PAGE analysis of the pellet from pulldown assays using soluble moesin-His and the cytoplasmic tail of CD44-GST (or NHERF1-GST) immobilized on beads. Moesin in the pellet is detected by anti-His antibody. CD44-GST (or NHERF1-GST) is detected by Coomassie Blue to verify equal loading. *B*, quantitation of the relative amounts of bound moesin determined by densitometry.

stabilization of binding of the FLAP to the FERM domain should reduce membrane association. Therefore we analyzed the structure to determine whether hydrophobic interactions could be enhanced by mutating a FLAP residue from a short side chain to a hydrophobic side chain. That analysis predicted that mutation of Gly-487 to valine would provide an additional hydrophobic interaction of a side chain to the FERM domain hydrophobic groove. As predicted, moesin protein with a G487V mutation showed decreased membrane localization (Fig. 8, *A* and *B*). Thus, these results show that hydrophobic interactions in this region are deleterious to membrane association and may explain why evolution has produced a low frequency of such residues in this region.

Now that we have introduced the concept of the FLAP, the findings with the K60N mutation in the pocket can be explained (Fig. 2). Analysis of the structure shows there is an electrostatic interaction between Lys-60 and Asp-472/Asp-474 in the FLAP. The K60N mutation would eliminate that interaction and facilitate release of the FLAP. Thus, enhanced membrane localization of K60N supports the concept that the FLAP is autoinhibitory.

FLAP Removal Enhances PIP2-induced Binding of Protein Ligands CD44 and NHERF1—The FLAP masks both the PIP2-POCKET and the hydrophobic groove to which the cytoplasmic tails of transmembrane proteins bind. We investigated the *in vitro* ligand binding properties of the ΔFLAP moesin (Fig. 9). ΔFLAP moesin resembles WT moesin in two fundamental ways. It bound poorly to the CD44 and NHERF1 tails in the absence of PIP2 (*i.e.* in the PS control) and its binding to the CD44 and NHERF1 tails was markedly enhanced in the presence of PIP2. These studies support two conclusions. First, deletion of the FLAP has not dramatically altered the conformation, which remains autoinhibited. Second, PIP2 is still required to open the protein. However, binding of the ΔFLAP moesin is not identical to WT moesin. It binds twice as much CD44 in the presence of PIP2 and 40% more NHERF1 (Fig. 9*B*). Thus removal of the FLAP has increased its ability to be activated by PIP2. This augmentation is likely to contribute to its enhanced localization at the membrane.

Evidence That PATCH and POCKET Do Not Bind PIP2 Simultaneously—We used two experimental approaches to distinguish whether binding of the two sites is simultaneous. First we assessed cooperativity of moesin binding to PIP2, if both sites are involved simultaneously the shape of the curve of PIP2 concentration dependence should be sigmoidal. In this assay we held constant the mass fraction of the total lipid concentration (and thus LUVs concentration) while we varied the mass fraction of PIP_2. We measured the binding of moesin to 0.28 mM accessible total lipid containing variable concentration (0–15%) of PIP_2 (Fig. 11*A*). We observed a monotonic hyperbolic increase in the binding curve, indicating a noncooperative mode of binding of moesin to PIP2. These results are comparable with the noncooperative binding of ezrin to PIP2 (25).

An independent approach to determine whether both sites bind PIP2 simultaneously is to determine the stoichiometry of binding of moesin to PIP2 in membrane. To do so we quantitated the binding of moesin to PIP2 on membrane surfaces using a well established protein to membrane fluorescence resonance energy transfer (FRET) assay (26). The LUVs used contained a high PIP2 concentration (10 mol %) of PIP2, to assure saturating moesin binding. Graded concentrations of LUVs were added to fixed amounts of moesin. Binding (*i.e.* FRET) increased linearly up to an inflection point where all moesin was bound and binding was not increased as further lipid was added. Calculation of stoichiometry from five experiments indicated an average ± S.E. of 0.86 ± 0.07 PIP2 molecules per moesin molecule. These data appear inconsistent with conventional models involving sustained simultaneous binding of two PIP2 molecules to moesin. Instead, we favor a model of progressive activation by a single PIP2 molecule first binding transiently to the PATCH and then stably to the POCKET, as described at the end of the discussion.

DISCUSSION

Two PIP2-binding sites have been described on the ERM protein but knowledge about them has not provided a coherent molecular mechanism for ERM protein activation. The present study provides additional characterization of both sites and of an autoinhibitory FLAP, which masks one of the sites. We propose a model of ERM activation in which PIP2 first binds to the PATCH, releases the FLAP by electrostatic repulsion (and other conformational mechanisms), exposing the POCKET. PIP2 binding to the POCKET then replaces PIP2 binding to the PATCH, which completes activation of ERM.

POCKET—Three lysines in the POCKET were predicted from the crystal structure of the IP3-FERM complex to contribute to PIP2 binding in the FERM domain. Our mutational analysis shows that only two (Lys-63 and Lys-278) are critical in full-length moesin. This confirms and extends the previous mutational analysis of the FERM domain showing that combined mutation of Lys-63 and an adjacent residue impairs FERM domain binding to PIP2 (17). In light of the lack of contribution of Lys-60, it is likely that the orientation of the headgroup of membrane PIP2 bound in this POCKET is not exactly identical to that of bound IP3 in the structure. PIP2 is inserted in the membrane by its fatty acids; its headgroup has major binding constraints that are irrelevant to IP3 (30). Furthermore, the 1-phosphate that provides linkage to the glycerol backbone is spatially constrained in PIP2 and therefore binding of Lys-60 to the 1-phosphate of IP3 as shown in the structure is unlikely to be possible with PIP2 (30).

Based on the crystal structure, the conformation change induced by PIP2 binding to the POCKET was proposed to release the autoinhibitory C terminus and thereby activate ERM (16). Our studies provide the first experimental validation that this POCKET (Lys-63 and Lys-278) is critical for ERM binding to the membrane (Fig. 2) and for the PIP2-induced conformational release of autoinhibition (Fig. 3).

Autoinhibitory FLAP Region—The POCKET was identified in the solved structure of an isolated FERM domain in which there is no obstruction of access to the POCKET (16). However, the subsequently solved structure of full-length autoinhibited ERM showed that the POCKET is inaccessible (7) because it is overlaid by a linker region. We call this linker the FLAP and characterize it in the present studies. An earlier structure of the FERM domain in a swapped dimer showed that residues 488–494 (the C-terminal part of the FLAP) bound to FERM and suggested the same mode of binding in the autoinhibited monomer (8). The FLAP masks the PIP2-binding POCKET (Fig. 1*B*, *site 2*) and the hydrophobic groove to which tails of transmembrane proteins (like CD44, CD43 etc.) bind (Fig. 1*B*, *site 3*).

Our choice of the name FLAP is based on its properties. First, the FLAP is rich in acidic residues. Second, the region is loosely bound to the FERM domain. It has extremely limited hydrophobic interaction with the underlying hydrophobic groove of the FERM domain. We demonstrate that this hydrophobic association is finely tuned because a single mutation to decrease it (L281A) markedly enhances membrane association and a single mutation to increase it (G278V) markedly diminishes membrane association (Fig. 8). It is flexible due to the presence of numerous small residues (Ala, Ser, and Gly) (Fig. 7). Furthermore, it can act as a FLAP because its "tip" is so poorly bound that it is not resolved in the structure. Only its "base" or "hinge" provided by N-terminal and C-terminal sequence is more tightly bound to the FERM domain (Fig. 7*A*).

PATCH—The positive surface potential of the region surrounding the PATCH is the most favorable region of autoinhibited moesin for interaction with the negatively charged inner leaflet of the plasma membrane (Fig. 4*A*). Previous mutational analysis showed that simultaneous mutation of four lysines in this region destroyed PIP2 binding and membrane localization (17). We showed that even single mutations in the PATCH interfered with the membrane localization and the successful opening of autoinhibited ERM. Our data demonstrate that the PATCH as well as the POCKET are required for the activation of ERM. But a notable difference between the two sites relates to their accessibility to PIP2 in autoinhibited moesin. Only the PATCH is a candidate for binding of autoinhibited moesin to PIP2 because of its availability and its favorable surface potential. In contrast, the binding of PIP2 to the POCKET in autoinhibited moesin is unfavorable because it is covered by the FLAP. The FLAP not only is a steric hindrance for PIP2 access to the POCKET, but also the strong negative charge of the FLAP reverses the positive electrostatic potential around the POCKET (Fig. 7).

We propose that the previously described electrostatic mechanism of "interfacial activation" is an attractive one to facilitate release of the FLAP when moesin binds to membrane PIP2 via the PATCH. Harden and Sondek (31) have described interfacial activation as a mechanism for activation of PLC enzymes. Most PLC enzymes are autoinhibited by a linker that occludes their PIP2-binding site (*i.e.* the catalytic cleft). The PLC linker is poorly conserved but has a high abundance of negatively charged residues. When PLC is brought to the membrane by any of several different recruitment mechanisms, the electrostatic repulsion by negative charge on the inner leaflet of the membrane pushes the negatively charged PLC linker out of the cleft (32). They coined the term interfacial activation to describe this electrostatic release. The FLAP in moesin shares

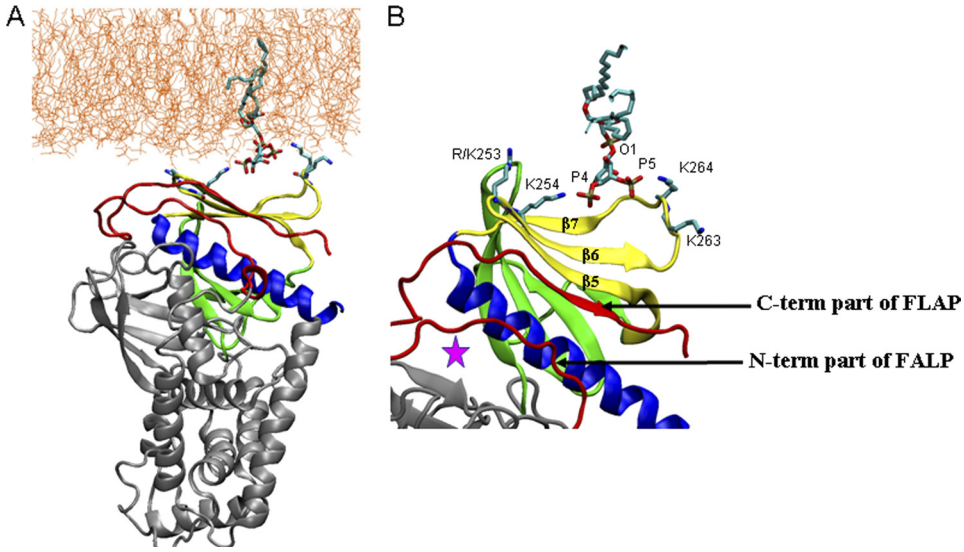

FIGURE 10. **Representation of a proposed additional mechanism for conformational change when PIP2 binds to the PATCH.** *Panel A* shows a model of the PATCH of intact ERM interacting with a lipid bilayer including a PIP2 molecule. Lobe C, the PH-like domain, has been colored to facilitate visualization: β1–β4 strands in *green*, β5–β7 strands in *yellow*, and the α-helix in *blue*. The FLAP is colored *red*. The headgroup of PIP2 is accommodated between the two pairs of lysines (Lys-253/Lys-254 and Lys-262/Lys-263) whose side chains are shown in ball and stick representation. *Panel B* is a magnified view of the binding site.

the four key properties of the PLC-linker: highly negatively charged, loosely bound, flexible, and occluding the PIP2-binding site. We propose that binding of PIP2 to the PATCH promotes release of the FLAP by the same kind of interfacial activation.

Possible Additional Mechanism of Conformational Activation of ERM at the Plasma Membrane—Conformation changes in the POCKET are required to accommodate PIP2 because its conformation in the autoinhibited moesin is not optimal for binding PIP2. The first evidence for this comes from comparisons by Hamada and colleagues (16) who showed that aspects of the FERM domain conformation are altered when the tail is released, including changes that make the POCKET more suitable for IP3 binding. Our structural comparison between the FERM domain in full-length autoinhibited moesin and free FERM domain support this observation (supplemental Fig. S2). Namely removal of the tail and FLAP caused major displacement of the whole region containing the PATCH residues (β sheets β5/β6/β7) and even some displacement of α1C helix, which contains the key POCKET residue Lys-278. Such conformational changes in C-lobe widen the cleft between lobes A and C and therefore facilitate accommodation of PIP2 in the POCKET.

We propose the possibility that PIP2 binding to the PATCH promotes a conformational change similar to that described in the previous paragraph. The distinctive structure of the PIP2-binding site in the PATCH is well suited to induce a conformation change in the FERM domain (Fig. 10). Two key structural features of ERM protein support this model. 1) The two critical pairs of lysines (Lys-253/Lys-254 and Lys-262/Lys-263) are on flexible loops (β5–β6) and (β6–β7), preceding and following the β6 strand in the PH-like domain. The pairs form a pocket with geometry generally appropriate to accommodate the headgroup of PIP2. Because loops are typically flexible, these residues (and their side chains) can adjust their position to simultaneously bind to the 4- and 5-phosphoryl groups of PIP2. 2) As those interactions progress, they will destabilize binding of the FLAP by the following mechanism. In autoinhibited moesin the C-terminal part of the FLAP (Fig. 7*C*) is a β strand that is hydrogen bonded to strand β5 becoming a fourth strand in the β5/β6/β7 β sheet typical of PH domains (Fig. 7*C*). The simultaneous force from the PIP2-binding loops on either side of the β6 strand would be expected to cause deformation of β6, causing distortion of the β sheet (β5/β6/β7). As the β sheet is distorted, the coordination of the C-terminal part of the FLAP with β5 is impaired. The result will not be only release of the FLAP and unmasking the POCKET, but also helping release the tail and widening the cleft between lobes A and C (similar to the mechanism proposed by Hamada *et al.* (16)).

One characteristic of our experimental data fits especially well with this model, namely that mutation of single lysine residues in the PATCH seriously impairs release of autoinhibition (and membrane localization) but has a limited affect on PIP2 binding *per se*. Mutation of a single residue would be expected to seriously impair this specialized release mechanism in which strong distortion of each of the loops is critical. In contrast in various other mechanisms (such as the electrostatic mechanism) mutations of single residues would not necessarily be critical (unless they impaired PIP2 binding).

PIP2 Interaction and ERM Phosphorylation—In the absence of PIP2, the C-terminal phosphorylation is virtually impossible because the site is close enough to the FERM domain that it does not leave enough room for a phosphoryl group (8) and tail binding to FERM is so thermodynamically stable that phosphorylation is effectively prevented (15, 33). The final role of PIP2 in activating the ERM protein is binding to the POCKET, which completes the conformational activation initiated by PIP2 binding to the PATCH and relaxes binding of the C-terminal tail to the FERM domain (as proposed by Hamada and colleagues (16)). This relaxation provides access of the tail phosphorylation site to ERM kinases, which can be abundant in the vicinity of the plasma membrane (34). Thus, phosphoryla-

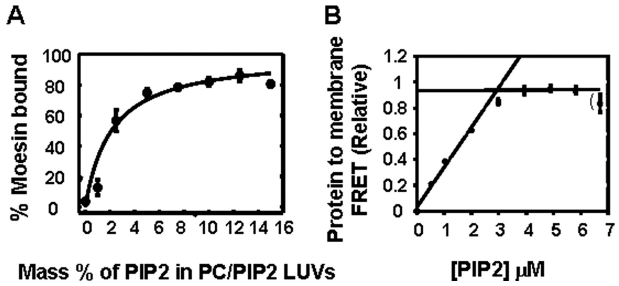

FIGURE 11. **Analysis of stoichiometry and cooperativity of moesin binding to PIP2.** *A,* cooperativity. Binding of moesin-Alexa 488 to LUVs composed of varying percentages (0–15%) of PIP_2 assessed by co-sedimentation assays followed by spectrofluorimetric analysis. LUVs having fixed total lipid concentration (0.28 mM accessible lipid) but vary in their mole fractions of PIP2 were added to a fixed concentration of moesin-Alexa 488 (0.4 μM). The percent of moesin bound is plotted as a function of the percentage of PIP_2 in the LUVs where each point is the average of two experiments. The *solid line* is the nonlinear least squares best fit of all the data. *B,* stoichiometry. A standard protein to membrane FRET assay was employed to quantitate membrane-bound moesin. The FRET measured occurs between intrinsic tryptophan donors in moesin and the dansyl-PE acceptors in the LUVs. LUVs containing 10 mol % PIP2 in a lipid mixture mimicking the plasma membrane inner leaflet (PE/PC/PS/L-α-phosphatidylinositol/sphingomyelin/cholesterol/dansyl-PE/PIP2 (23.8:9.1:18.1:4.5:4.5:25:5:10)) were titrated into a fixed concentration of nonlabeled moesin (3.6 μM). These conditions were chosen to drive high affinity PIP2 binding such that the titration yields a linear increase in membrane-associated moesin until all proteins had been bound and a plateau achieved. High variability (a time dependent signal loss we ascribe to vesicle aggregation) was observed when LUV concentrations exceeded 6.0 μM PIP2 (data point shown in *parentheses*). The intersection of the best-fit straight lines for the linear increase and plateau regions represent the saturation point, yielding 3.1 ± 0.25 μM PIP2 molecules per 3.6 μM moesin molecules equivalent to a PIP2/moesin ratio of about 0.86 ± 0.07 (average of 5 experiments ± S.E.).

tion is facilitated by PIP2 binding as suggested by Fievet *et al.* (15). Phosphorylation at the threonine site creates an electrostatic repulsion between the C-terminal tail and the FERM domain, thereby stabilizing the open state of ERM molecule (8).

Evidence for Sequential Rather Than Simultaneous PIP2 Binding to Two Sites—These studies document that the PATCH and the POCKET are two distinct but essential PIP2-binding sites on the FERM domain and characterize the FLAP as an important autoinhibitory region that masks the initial access to the POCKET. Thus ERM proteins have evolved a two-site mechanism for conformational activation by PIP2. A critical related question is whether these two PIP2-binding sites: (*a*) bind simultaneously to two PIP2 molecules or (*b*) bind sequentially to individual PIP2 molecule. Both published data and our new data (Fig. 11) indicate that the two sites do NOT bind simultaneously to two molecules of PIP2. First, PIP2 binds to moesin in a concentration-dependent manner, characteristic of interaction with a single PIP2 molecule, not two PIP2 molecules (Fig 11*A*); this is consistent with published findings for ezrin (25). Second, under the saturation phase of binding, only one molecule of PIP2 binds to one molecule of moesin (Fig 11*B*). This is consistent with previous studies showing that ERM protein binding to PIP2 does not induce the clustering of PIP2 molecules (25). Third, our structural analysis fails to identify any orientation of the FERM domain, which allows simultaneous binding of the PATCH and POCKET to two PIP2 molecules in a planar membrane.

We propose a conceptual model that incorporates the knowledge that moesin has two PIP2-binding sites that do not bind PIP2 simultaneously. The key concept is that PIP2 binds transiently to one site (the PATCH) and then stably to the other site (the POCKET). Initially a molecule of PIP2 binds to the PATCH (the most favorable electrostatically on closed ERM). But this binding to the PATCH is *transient* and persists only long enough to induce conformational changes (including release of FLAP), which are necessary to expose the POCKET. The exposed POCKET has stronger attraction than the PATCH for the negatively charged lipids in the membrane and especially for PIP2. These forces will contribute to attraction of the molecular region surrounding the POCKET toward the inner leaflet of the membrane. This results in rotation of the entire FERM domain causing the PATCH to tilt away from the plasma membrane. As a result, the transient binding of PIP2 to the PATCH is now lost and is replaced by stable PIP2 binding to the POCKET. We favor the possibility that the same PIP2 molecule binds transiently to the PATCH then migrates to the final binding site, the POCKET, resulting in a progressive conformational activation of ERM. This model is similar to the mechanism by which the same ATP molecule binds to three different binding sites on the surface of subunit B of *Methanosarcina mazei* Gö A_1A_0 ATP synthase with a stoichiometry of 1:1. The first binding of the ATP molecule to site 1 induces conformational changes promoting binding of subunit F to subunit B, which induces migration of the ATP to its final binding pocket via transitional intermediates on the surface of subunit B (35). This strategy that has been evolved by ERM proteins provides a progressive mechanism for activation by PIP2. Its functional design avoids requiring very high PIP2 concentrations that would be necessary for a mechanism requiring simultaneous occupancy of two PIP2 molecules.

Acknowledgment—We thank Dr. Tamas Balla for informative discussions. We thank Dr. Richard Pastor and Dr. Richard Venable for providing the lipid bilayer structures and for helpful discussions.

REFERENCES

1. Hughes, S. C., and Fehon, R. G. (2007) Understanding ERM proteins. The awesome power of genetics finally brought to bear. *Curr. Opin. Cell Biol.* **19,** 51–56
2. Niggli, V., and Rossy, J. (2008) Ezrin/radixin/moesin, versatile controllers of signaling molecules and of the cortical cytoskeleton. *Int. J. Biochem. Cell Biol.* **40,** 344–349
3. Bretscher, A., Edwards, K., and Fehon, R. G. (2002) ERM proteins and merlin. Integrators at the cell cortex. *Nat. Rev. Mol. Cell Biol.* **3,** 586–599
4. Fiévet, B., Louvard, D., and Arpin, M. (2007) ERM proteins in epithelial cell organization and functions. *Biochim. Biophys. Acta* **1773,** 653–660
5. Mori, T., Kitano, K., Terawaki, S., Maesaki, R., Fukami, Y., and Hakoshima, T. (2008) Structural basis for CD44 recognition by ERM proteins. *J. Biol. Chem.* **283,** 29602–29612
6. Reczek, D., and Bretscher, A. (1998) The carboxyl-terminal region of EBP50 binds to a site in the amino-terminal domain of ezrin that is masked in the dormant molecule. *J. Biol. Chem.* **273,** 18452–18458
7. Li, Q., Nance, M. R., Kulikauskas, R., Nyberg, K., Fehon, R., Karplus, P. A., Bretscher, A., and Tesmer, J. J. (2007) Self-masking in an intact ERM-merlin protein. An active role for the central α-helical domain. *J. Mol. Biol.* **365,** 1446–1459
8. Pearson, M. A., Reczek, D., Bretscher, A., and Karplus, P. A. (2000) Structure of the ERM protein moesin reveals the FERM domain fold masked by an extended actin binding tail domain. *Cell* **101,** 259–270
9. Kunda, P., Pelling, A. E., Liu, T., and Baum, B. (2008) Moesin controls

cortical rigidity, cell rounding, and spindle morphogenesis during mitosis. *Curr. Biol.* **18,** 91–101
10. Nakamura, F., Amieva, M. R., and Furthmayr, H. (1995) Phosphorylation of threonine 558 in the carboxyl-terminal actin-binding domain of moesin by thrombin activation of human platelets. *J. Biol. Chem.* **270,** 31377–31385
11. Roch, F., Polesello, C., Roubinet, C., Martin, M., Roy, C., Valenti, P., Carreno, S., Mangeat, P., and Payre, F. (2010) Differential roles of PtdIns(4,5)P_2 and phosphorylation in moesin activation during *Drosophila* development. *J. Cell Sci.* **123,** 2058–2067
12. Hirao, M., Sato, N., Kondo, T., Yonemura, S., Monden, M., Sasaki, T., Takai, Y., Tsukita, S., and Tsukita, S. (1996) Regulation mechanism of ERM (ezrin/radixin/moesin) protein/plasma membrane association. Possible involvement of phosphatidylinositol turnover and Rho-dependent signaling pathway. *J. Cell Biol.* **135,** 37–51
13. Yonemura, S., Matsui, T., Tsukita, S., and Tsukita, S. (2002) Rho-dependent and -independent activation mechanisms of ezrin/radixin/moesin proteins. An essential role for polyphosphoinositides *in vivo*. *J. Cell Sci.* **115,** 2569–2580
14. Hao, J. J., Liu, Y., Kruhlak, M., Debell, K. E., Rellahan, B. L., and Shaw, S. (2009) Phospholipase C-mediated hydrolysis of PIP2 releases ERM proteins from lymphocyte membrane. *J. Cell Biol.* **184,** 451–462
15. Fievet, B. T., Gautreau, A., Roy, C., Del Maestro, L., Mangeat, P., Louvard, D., and Arpin, M. (2004) Phosphoinositide binding and phosphorylation act sequentially in the activation mechanism of ezrin. *J. Cell Biol.* **164,** 653–659
16. Hamada, K., Shimizu, T., Matsui, T., Tsukita, S., and Hakoshima, T. (2000) Structural basis of the membrane-targeting and unmasking mechanisms of the radixin FERM domain. *EMBO J.* **19,** 4449–4462
17. Barret, C., Roy, C., Montcourrier, P., Mangeat, P., and Niggli, V. (2000) Mutagenesis of the phosphatidylinositol 4,5-bisphosphate (PIP2) binding site in the NH_2-terminal domain of ezrin correlates with its altered cellular distribution. *J. Cell Biol.* **151,** 1067–1080
18. Ingley, E., and Hemmings, B. A. (1994) Pleckstrin homology (PH) domains in signal transduction. *J. Cell. Biochem.* **56,** 436–443
19. Balaji, S., Babu, M. M., Iyer, L. M., and Aravind, L. (2005) Discovery of the principal specific transcription factors of Apicomplexa and their implication for the evolution of the AP2-integrase DNA binding domains. *Nucleic Acids Res.* **33,** 3994–4006
20. Cozier, G. E., Carlton, J., Bouyoucef, D., and Cullen, P. J. (2004) Membrane targeting by pleckstrin homology domains. *Curr. Top. Microbiol. Immunol.* **282,** 49–88
21. Lemmon, M. A., and Ferguson, K. M. (2001) Molecular determinants in pleckstrin homology domains that allow specific recognition of phosphoinositides. *Biochem. Soc. Trans.* **29,** 377–384
22. Balla, T. (2005) Inositol-lipid binding motifs. Signal integrators through protein-lipid and protein-protein interactions. *J. Cell Sci.* **118,** 2093–2104
23. Patino-Lopez, G., Aravind, L., Dong, X., Kruhlak, M. J., Ostap, E. M., and Shaw, S. (2010) Myosin 1G is an abundant class I myosin in lymphocytes whose localization at the plasma membrane depends on its ancient divergent pleckstrin homology (PH) domain (Myo1PH). *J. Biol. Chem.* **285,** 8675–8686
24. Hokanson, D. E., Laakso, J. M., Lin, T., Sept, D., and Ostap, E. M. (2006) Myo1c binds phosphoinositides through a putative pleckstrin homology domain. *Mol. Biol. Cell* **17,** 4856–4865
25. Blin, G., Margeat, E., Carvalho, K., Royer, C. A., Roy, C., and Picart, C. (2008) Quantitative analysis of the binding of ezrin to large unilamellar vesicles containing phosphatidylinositol 4,5-bisphosphate. *Biophys. J.* **94,** 1021–1033
26. Lai, C. L., Landgraf, K. E., Voth, G. A., and Falke, J. J. (2010) Membrane docking geometry and target lipid stoichiometry of membrane-bound PKCα C2 domain. A combined molecular dynamics and experimental study. *J. Mol. Biol.* **402,** 301–310
27. Amieva, M. R., Litman, P., Huang, L., Ichimaru, E., and Furthmayr, H. (1999) Disruption of dynamic cell surface architecture of NIH3T3 fibroblasts by the N-terminal domains of moesin and ezrin. *In vivo* imaging with GFP fusion proteins. *J. Cell Sci.* **112,** 111–125
28. Finnerty, C. M., Chambers, D., Ingraffea, J., Faber, H. R., Karplus, P. A., and Bretscher, A. (2004) The EBP50-moesin interaction involves a binding site regulated by direct masking on the FERM domain. *J. Cell Sci.* **117,** 1547–1552
29. Morales, F. C., Takahashi, Y., Momin, S., Adams, H., Chen, X., and Georgescu, M. M. (2007) NHERF1/EBP50 head-to-tail intramolecular interaction masks association with PDZ domain ligands. *Mol. Cell. Biol.* **27,** 2527–2537
30. Li, Z., Venable, R. M., Rogers, L. A., Murray, D., and Pastor, R. W. (2009) Molecular dynamics simulations of PIP_2 and PIP_3 in lipid bilayers. Determination of ring orientation, and the effects of surface roughness on a Poisson-Boltzmann description. *Biophys. J.* **97,** 155–163
31. Harden, T. K., and Sondek, J. (2006) Regulation of phospholipase C isozymes by *ras* superfamily GTPases. *Annu. Rev. Pharmacol. Toxicol.* **46,** 355–379
32. Hicks, S. N., Jezyk, M. R., Gershburg, S., Seifert, J. P., Harden, T. K., and Sondek, J. (2008) General and versatile autoinhibition of PLC isozymes. *Mol. Cell* **31,** 383–394
33. Jayaraman, B., and Nicholson, L. K. (2007) Thermodynamic dissection of the Ezrin FERM/CERMAD interface. *Biochemistry* **46,** 12174–12189
34. Belkina, N. V., Liu, Y., Hao, J. J., Karasuyama, H., and Shaw, S. (2009) LOK is a major ERM kinase in resting lymphocytes and regulates cytoskeletal rearrangement through ERM phosphorylation. *Proc. Natl. Acad. Sci. U.S.A.* **106,** 4707–4712
35. Raghunathan, D., Gayen, S., Kumar, A., Hunke, C., Gruber, G., and Verma, C. S. (2012) *J. Bioenerg. Biomembr.* **44,** 213–224

Cell Biology:

Activation of Moesin, a Protein That Links Actin Cytoskeleton to the Plasma Membrane, Occurs by Phosphatidylinositol 4,5-bisphosphate (PIP2) Binding Sequentially to Two Sites and Releasing an Autoinhibitory Linker

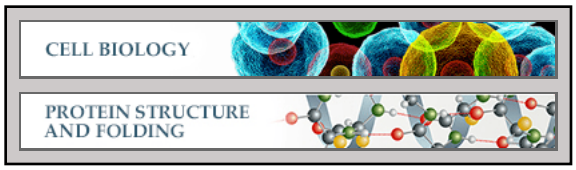

Khadija Ben-Aissa, Genaro Patino-Lopez, Natalya V. Belkina, Ofelia Maniti, Tilman Rosales, Jian-Jiang Hao, Michael J. Kruhlak, Jay R. Knutson, Catherine Picart and Stephen Shaw

J. Biol. Chem. 2012, 287:16311-16323.
doi: 10.1074/jbc.M111.304881 originally published online March 20, 2012
